

# Valid data based normalized cross-correlation (VDNCC) for topography identification

Mingsi Tong<sup>a,b</sup>, Yunlu Pan<sup>a</sup>, Zhan Li<sup>b</sup>, Weiyang Lin<sup>a,b,\*</sup>

<sup>a</sup> Key Laboratory of Micro-systems and Micro-structures Manufacturing of Ministry of Education, School of Mechatronics Engineering, Harbin Institute of Technology, Harbin 150001, China

<sup>b</sup> Research Institute of Intelligent Control and Systems, Harbin Institute of Technology, Harbin 150001, China

## ARTICLE INFO

### Article history:

Received 29 January 2018

Revised 13 April 2018

Accepted 27 April 2018

Available online 4 May 2018

### Keywords:

Normalized cross-correlation (NCC)

Ballistics identification

Topography identification

Pattern recognition

## ABSTRACT

The Normalized Cross-Correlation (NCC) function is a widely used pattern-matching method. However, when the input data have a void area created by non-rectangular data or outliers, the accuracy of the standard NCC function may decrease. Especially when the regional mean values under the NCC window have a significant difference in the global mean value, the possible mis-matching may affect the identification results. In this paper, a valid data based NCC (VDNCC) algorithm is proposed for eliminating the effect of the void area. The new algorithm prevents void areas from being included in the calculation by introducing the valid data templates. VDNCC obtains higher NCC values and probabilities of correct matching in the experiments. In the ballistics identification tests, the results show that VDNCC can enhance the capacity of identification based on the NCC function as the core.

© 2018 Elsevier B.V. All rights reserved.

## 1. Introduction

Using computer technology to analyze or identify the images or topographies of ballistic toolmarks is a hotspot in the forensic field [1–5]. Computer technology can reduce the workload of forensic examiners and allow the comparing and tracing of thousands of firearms. Whether as a basic assisted analysis tool or an intelligent automatic identification method, most of these computer algorithms require a core matching function to match images or topographies. Although there are many matching methods in the machine vision field, the normalized cross-correlation (NCC) function based on statistics has been adopted by many ballistics studies [2–11], since the ballistic impressions originate from a random topography are difficult to be abstracted to enumerable or describable patterns. Thus, studying the matching process and improving the performance of the NCC algorithm has important significance in forensic identifications.

As a signal similarity metric method, the NCC function normalizes the result of cross-correlation into  $[-1,1]$ . The value of 1 means that the two input data are the same, while the value of  $-1$  means they are reversed. The NCC function scans the pattern on the reference data and calculates the correlation value at each position. In 1995, J. P. Lewis proposed a fast NCC algorithm based on fast Fourier transform (FFT) and a sum table to replace point-by-point calculations [12,13]. This algorithm significantly improves

the calculation efficiency and has become a classic NCC algorithm adopted by many mathematical tools and software libraries [14]. However, the NCC function has two limitations. The first limitation is that the arbitrary regional-matrix of the reference data must have similar mean values with the whole matrix. The second limitation is that the input data should be a full rectangular matrix, which means the dropouts, outliers or non-rectangular measured objects on the two compared data may affect the matching accuracy.

For the ballistics studies, the breech face impression and the firing pin impression on the primer of fired cartridge case are important evidences for ballistic identification, which is shown in Fig. 1. For the two impressions, the shapes of the useful areas are annular and round, respectively. However, the digitized matrix must be rectangular. Thus, the areas around the impression data are empty and usually marked as “void” or “null” by the computer. Furthermore, because of the limitation of the measuring instruments and the defects of the measured surface, the dropouts and outliers in the data are also filled with “void”. In this paper, the areas composed of the dropouts, outliers and other empty areas are defined as a void area. As shown in Fig. 2, the topographies contain large void areas produced by their non-rectangular shape and outliers from the measuring instruments. In this situation, the matching result will be affected by the inclusion of the void area.

In this paper, we proposed a new NCC algorithm which can reduce the negative effect of the void area on the NCC matching and improve the capacity of ballistic identification. The new algorithm was verified on a ballistic identification test, due to the breech face

\* Corresponding author.

E-mail address: [wylin@hit.edu.cn](mailto:wylin@hit.edu.cn) (W. Lin).

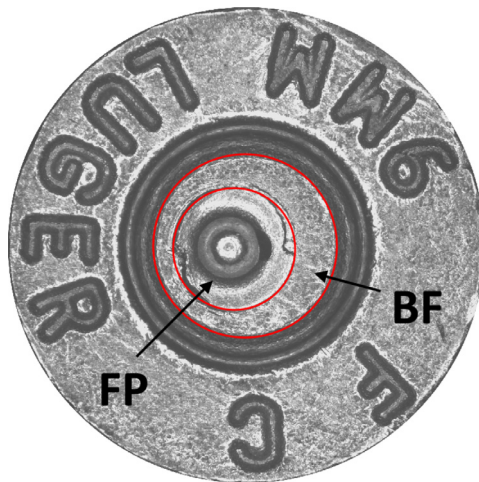


**Fig. 1.** The bottom of a fired cartridge case. Breech face impression (shown as BF) is the area between two red circles. FP indicates impression left by the firing pin. (For interpretation of the references to color in this figure legend, the reader is referred to the web version of this article.)

**Table 1**  
Test results of NCC for different void area sizes.

Percentage of void area	Central value	Global maximum value	Correct matching (Y/N)
0	0.61	0.60	Y
1/6	0.52	0.52	Y
2/6	0.39	0.47	N
3/6	0.34	0.48	N
4/6	0.26	0.48	N
5/6	0.16	0.48	N

**Table 2**

Compute time of point-by-point NCC and fast NCC (MATLAB code [14]) (Pattern matrix:  $150 \times 150$  points; Reference matrix:  $500 \times 500$  points; Environment: MATLAB 2016a, Intel E3 3.4 GHz, 16 GB RAM.).

NCC algorithm	Compute time
Point-by-point NCC	262.34 s
Fast NCC	0.09 s

impressions and the firing pin impressions contain a mass of void areas. The statistical experiment result shows that the new NCC algorithm can improve the capability of the NCC-based ballistic identification method.

## 2. The effect of the void area on the NCC result

In general applications, NCC calculations use a part of the candidate matrix as a pattern to scan the reference matrix and obtain an output matrix, which is composed of the NCC values of the pattern at each position of the reference. Let  $t(x, y)$  denote a pattern with  $N_x \times N_y$  points and  $f(x, y)$  denote a reference with  $M_x \times M_y$  points. As Reference [12], the NCC result can be calculated by

$$\gamma(u, v) = \frac{\sum_{x,y} (f(x, y) - \bar{f}_{u,v})(t(x - u, y - v) - \bar{t})}{\sqrt{\sum_{x,y} (f(x, y) - \bar{f}_{u,v})^2 \sum_{x,y} (t(x - u, y - v) - \bar{t})^2}} \quad (1)$$

where  $\sum_{x,y}$  represents  $\sum_{x=u}^{u+N_x-1} \sum_{y=v}^{v+N_y-1}$  for simplified writing;  $\bar{f}_{u,v}$  and  $\bar{t}$  are the mean values of  $f(x, y)$  and  $t(x, y)$  under the NCC window, which is generated by  $t(x, y)$ , respectively, as

$$\bar{f}_{u,v} = \frac{1}{N_x N_y} \sum_{x,y} f(x, y) \quad (2)$$

$$\bar{t} = \frac{\sum_{x,y} t(x - u, y - v)}{N_x N_y} \quad (3)$$

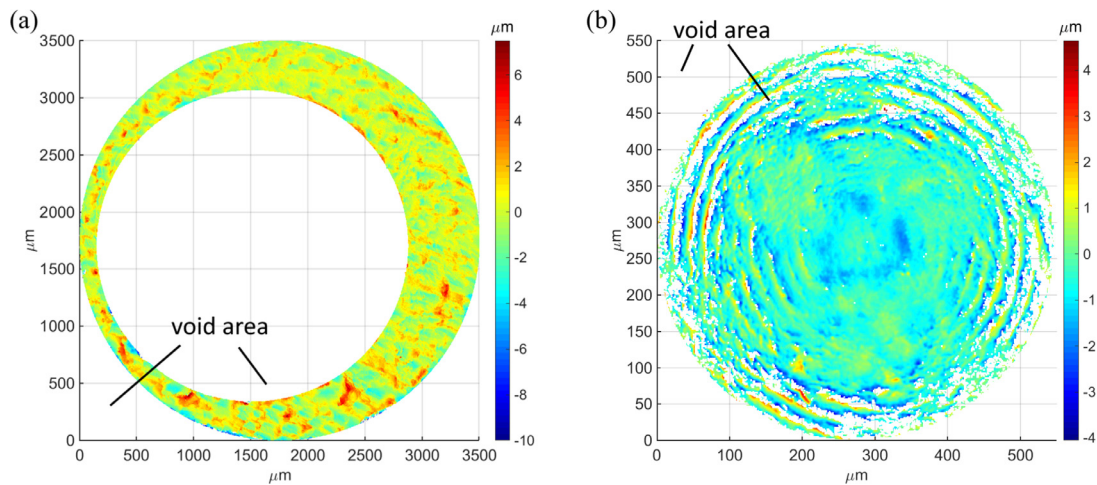


**Fig. 2.** The topographies of a breech face impression (a) and firing pin impression (b) on a primer of a cartridge case, which is treated with an areal spline filter [15].

**Table 3**

Test results of NCC based on overlapping data for different void area sizes.

Percentage of void area	Central value	Global maximum value	Correct matching (Y/N)
0	0.61	1	N
1/6	0.63	1	N
2/6	0.66	1	N
3/6	0.68	1	N
4/6	0.67	1	N
5/6	0.62	1	N

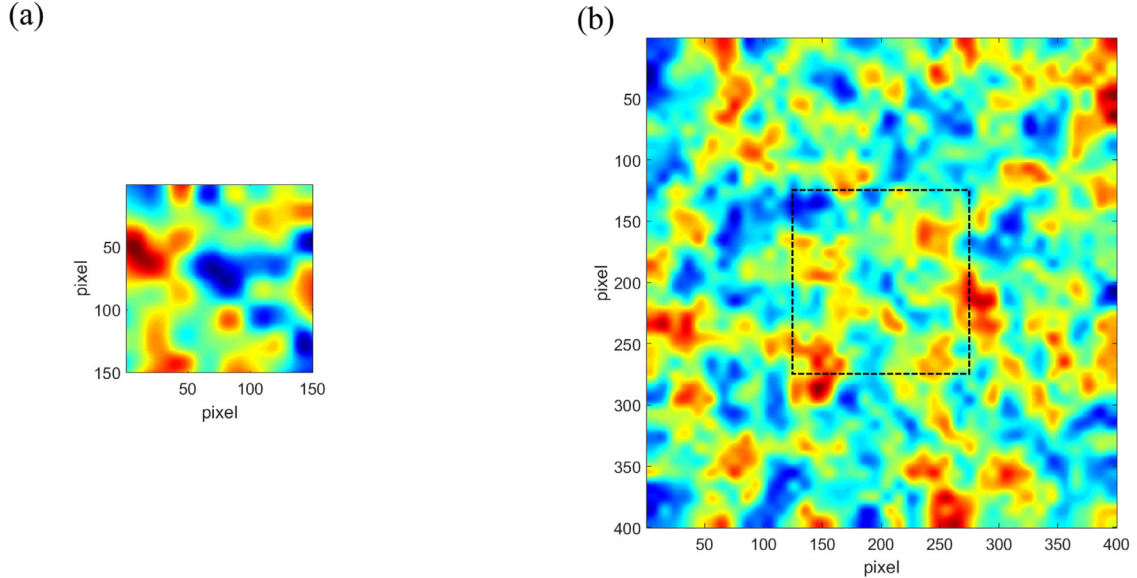


**Fig. 3.** Virtual random surfaces. Pattern (a) is similar to the center of the reference (b).

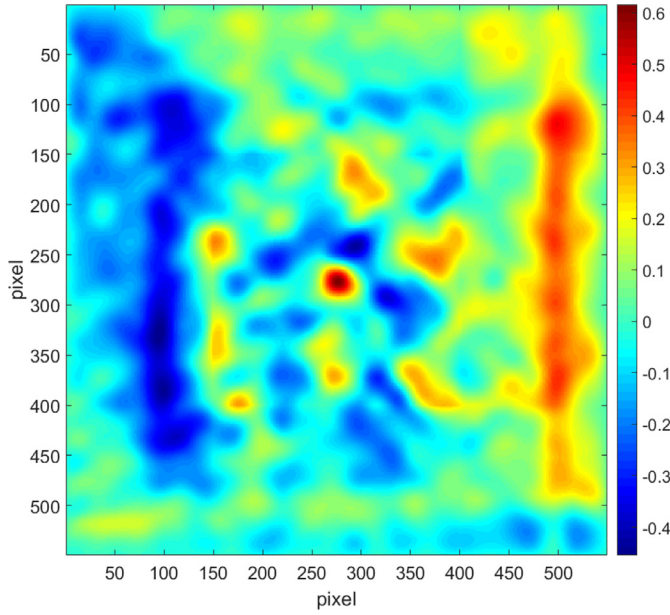


**Fig. 4.** The NCC result of the virtual random surfaces.

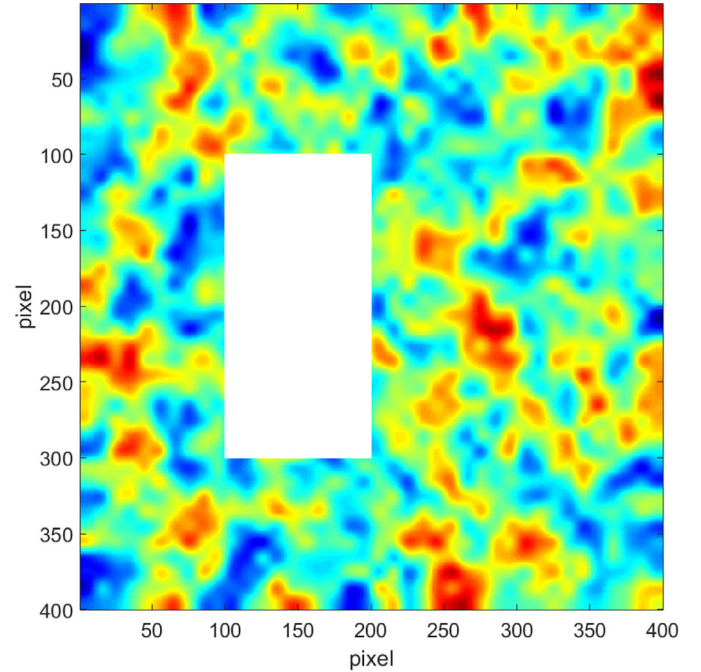


**Fig. 5.** The virtual random surface with the void area.

In Eqs. (2) and (3), each point at  $f(x, y)$  and  $t(x, y)$  under the NCC window is involved in the NCC calculation whether the point belongs to the void area or represents valid data [10]. The inclusion of the void areas without special treatment will seriously affect the correlation result. In fact, treating the void area is not a new challenge for the NCC function. When the NCC window oversteps the border of reference (e.g.,  $u > (M_x - N_x)$ ), the reference  $f(x, y)$  must be extended to fill the NCC window. This extended area can be considered the void area. For this situation, the common method requires filling the extended area with the mean value of  $f(x, y)$ , which is equivalent to pre-calculating  $f(x, y) - \bar{f}$  rather than the original  $f(x, y)$ .

However,  $\bar{f}_{u,v}$  in Eq. (1) is a regional mean value of reference  $f(x, y)$ . For practical applications, the regional mean value cannot ensure that the same value is maintained. When the regional mean

value deviates from the global mean value, the filling method does not work, and the effect of the void area is inevitable.

To illustrate the effect of the void area, a pair of virtual random surfaces are generated and are shown in Fig. 3. The sizes of the pattern and the reference surface are  $150 \times 150$  pixels and  $400 \times 400$  pixels. The pattern is similar to the center of the reference surface. Performing the NCC calculation on the two surfaces using Eq. (1), the maximum value of the resulting matrix is 0.61, which is located at the center, in the correct position, shown in Fig. 4.

A void area is added to the reference surface in Fig. 3(b), which contains 50% of the data corresponding to the pattern (shown in Fig. 5). Filling the void area with the mean value and performing the NCC calculation again, the maximum value of the output

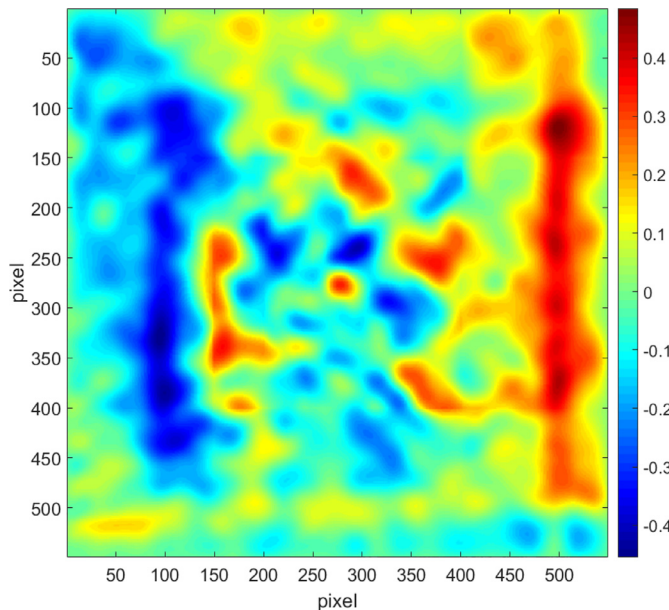


**Fig. 6.** The NCC result of the virtual random surface with the void area.

matrix declines to 0.48 (shown in Fig. 6). However, the NCC value at the center declines to 0.34, below the global maximum value, which indicates that the two surfaces cannot be matched correctly.

Table 1 lists the NCC results with different void area sizes. The experiment illustrates that the NCC values at the center decline when the void area increases. When the proportion of the void area is under 2/6, the global maximum NCC value is not located at the correct position. Thus, using the NCC function in firearm identifications without excluding the void area may result in misidentification.

### 3. Valid data based NCC function

To analyze the calculation of the NCC function, Fig. 7 is a schematic diagram of the NCC process. The two boxes represent the candidate sample and the reference sample and are overlapping in Fig. 7(a). The green pentagonal areas in the figure represent the valid areas, and the white areas are the void areas. When the NCC function calculates at the position shown in Fig. 7(a), all data points (the yellow area in Fig. 7(b)) under the NCC window are included in the denominator of Eqs. (2) and (3). This results in the effect of the void area on the output of the calculation, which is shown in Table 1. To reduce the effect of the void area, two NCC schemes can be proposed by modifying the calculation area.

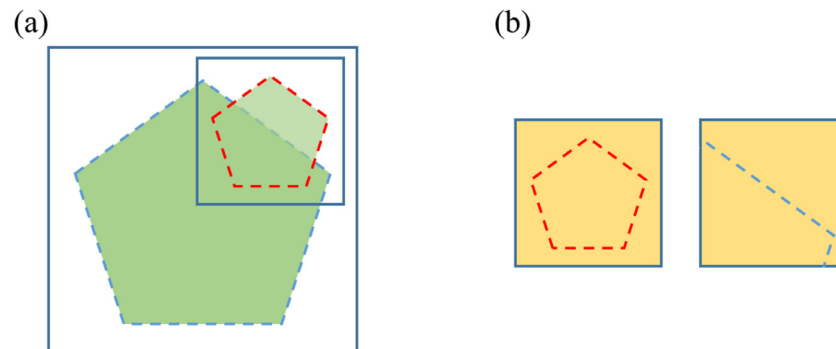


**Fig. 7.** Schematic diagram of standard NCC processing. When the NCC function is calculated at the position shown in (a), the data under the NCC window are shown in (b).

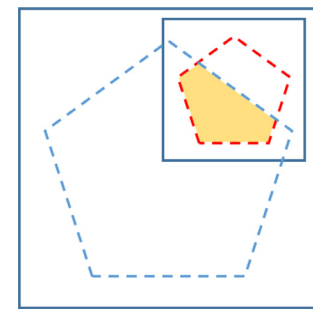


**Fig. 8.** Schematic diagram of NCC based on overlapping data. The yellow areas are the participants. (For interpretation of the references to color in this figure legend, the reader is referred to the web version of this article.)

The first scheme is calculating the overlap data of the valid area, eliminating all other areas, as shown in Fig. 8. This scheme can obtain higher similarity on the samples, which contain the void area, since the NCC result is based only on the overlap data. However, this scheme has two problems.

Firstly, with the shifting of the pattern, the form of the overlap area under the NCC windows is continually changing. Thus, the overlap areas have to be recalculated with every shift. Therefore, this scheme can only be calculated point by point instead of using the fast algorithm based on FFT [12], resulting in a calculation efficiency that is too low to be used in a massive ballistic comparison and search. Table 2 demonstrates the calculation costs of different NCC algorithms. There are three orders of magnitude between the compute time of the fast NCC and the point-by-point NCC.

Secondly, when the pattern shifts to the edge of the valid data, very few valid data points overlap. In this situation, the probability of a strong correlation of the overlapped data is very high, which results in the output matrix having abnormal values. Fig. 9 is the test result of this scheme. The NCC result of the center is approximately 0.61 closer to the result without the void area (Fig. 5). However, the fluctuation near the periphery is more notable than the central area, and the peak value can reach 1. Thus, this scheme has to restrict the overlap rate of the pattern on the reference, ensuring a sufficient overlap to avoid abnormal values. However, controlling the rate results in the waste of the valid data and creates difficulties in programming. Table 3 lists the test results of this scheme. In addition to the all-false matching results, the central value increased when the void area increased because only a part of the valid data overlapped, which produced unstable results, similar to what occurs on the edge.

The second scheme calculates the entire valid area, eliminating only the overlap of the void area (see Fig. 10). The non-overlapped valid data are included, which have been eliminated in the first scheme. In this scheme, when the pattern shifts to the edge, very

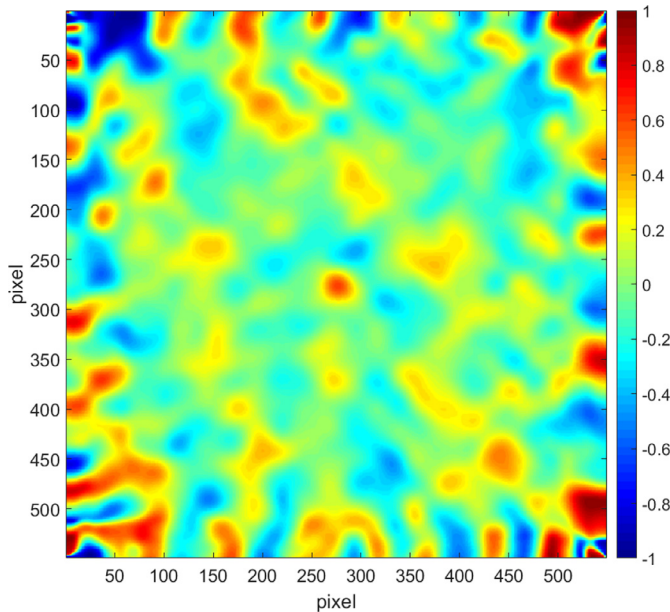


**Fig. 9.** Test result of NCC based on overlapping data.

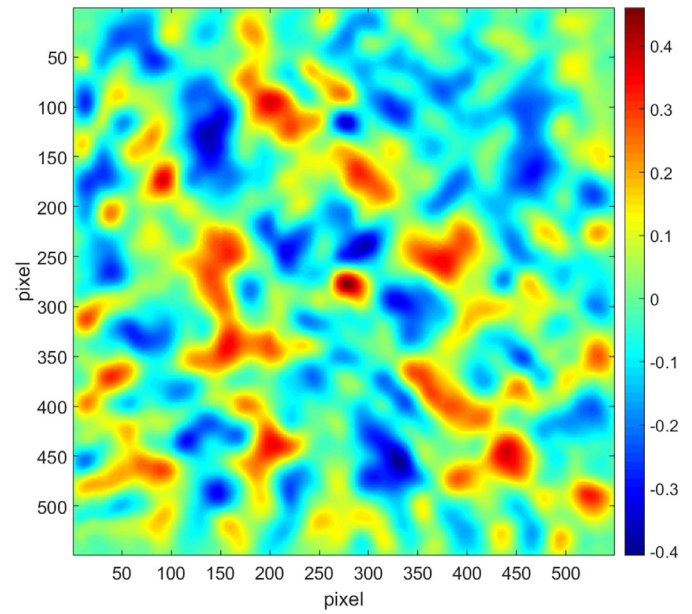


**Fig. 11.** Test result of NCC based on valid data.

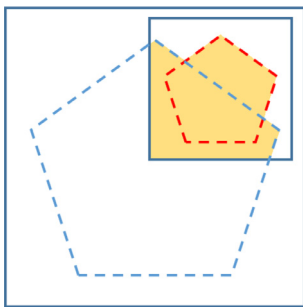


**Fig. 10.** Schematic diagram of NCC based on valid data.

**Table 4**  
Test results of NCC based on valid data for different void area sizes.

Percentage of void area	Central value	Global maximum value	Correct matching (Y/N)
0	0.60	0.60	Y
1/6	0.56	0.56	Y
2/6	0.46	0.46	Y
3/6	0.45	0.45	Y
4/6	0.38	0.38	Y
5/6	0.27	0.37	N

few data points are overlapping, and the denominators of Eqs. (2) and (3) are the sums of the valid points. The result is a weighted NCC value, and the proportion of overlapping points in the valid points is the weighting factor. The test result is shown in Fig. 11. The correct and unique peak is located at the center; other areas maintain relatively low and uniform values. Table 4 shows the test results of the second scheme with different void area sizes. Compared with Table 1, the value is higher than the results of standard NCC with the same void size, and it can tolerate a larger void area and match the samples correctly.

For a ballistics instance, Fig. 12(a) is a pattern from a candidate breech face impression on a primer of cartridge case; Fig. 12(b) is a known-matching reference impression, which should match the pattern at the position of the red box. Fig. 13 shows the correlation results of the standard NCC, the first NCC scheme based

**Table 5**  
Comparison of the three NCC algorithms for breech face matching.

Algorithms	Value in correct position	Global maximum value	Correct matching (Y/N)
Standard NCC	0.44	0.46	N
Overlapping data based NCC	0.52	1	N
Valid data based NCC	0.49	0.49	Y

on overlapping data and the second NCC scheme based on valid data. Whether the global maximum NCC value could appear at the correct position is the key indicator for the ballistic identification, since each pattern correlation should provide a NCC value and the position of this value. In a pair of two images, if the global maximum NCC value appear at the correct position, the shifts of the positions of all pattern correlations should be congruent. Table 5 shows the NCC value of the position of the pattern that should be matched and the global maximum NCC value. The results indicate that the second scheme is the only algorithm to match the pattern directly and correctly in these three NCC algorithms.

In contrast, the second scheme is more appropriate for matching non-full filled samples, such as firing pin and breech face impressions. In this paper, we named the second scheme VDNCC (valid data based NCC). In the following sections, the VDNCC algorithm will be discussed.

#### 4. The algorithm of VDNCC

The basic idea of VDNCC is to exclude overlapped void points. Thus, the valid data templates  $mt(x, y)$  and  $mf(x, y)$  are introduced into the NCC calculation:

$$\begin{cases} mf(x, y) = 1, & \text{when } f(x, y) \text{ is valid point} \\ mf(x, y) = 0, & \text{when } f(x, y) \text{ is void point} \end{cases} \quad (4)$$

$$\begin{cases} mt(x, y) = 1, & \text{when } t(x, y) \text{ is valid point} \\ mt(x, y) = 0, & \text{when } t(x, y) \text{ is void point} \end{cases} \quad (5)$$

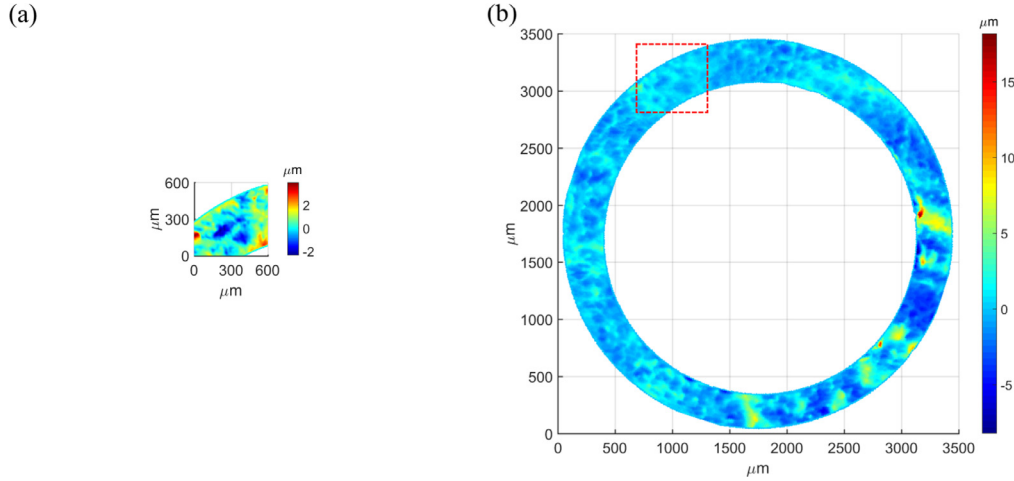


**Fig. 12.** A breech face pattern (a) and the reference impression (b) are known to match at the red box. (For interpretation of the references to color in this figure legend, the reader is referred to the web version of this article.)

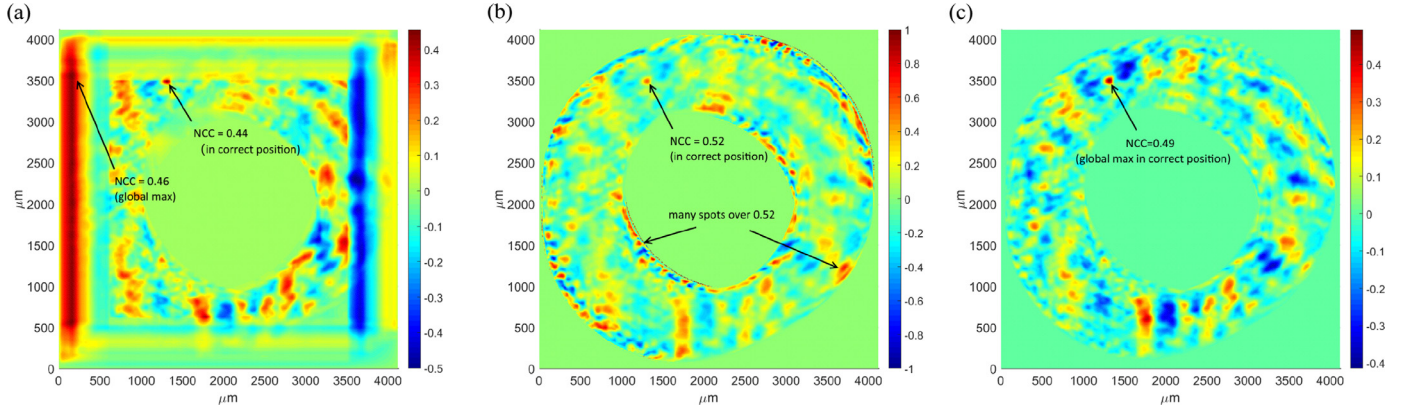


**Fig. 13.** Correlation results of the three NCC algorithms. (a) is the standard NCC; (b) is the overlapping data based NCC; (c) is the valid data based NCC.

Then, the VDNCC function can be expressed as:

$$\gamma(u, v) = \frac{\sum_{x,y} (f' - \bar{f}'_{u,v})(t' - \bar{t}')}{\sqrt{\sum_{x,y} (f' - \bar{f}'_{u,v})^2 \sum_{x,y} (t' - \bar{t}')^2}} \quad (6)$$

where

$$f' = f(x, y)mf(x, y)$$

$$\bar{f}'_{u,v} = \frac{\sum_{x,y} f'}{\sum_{x,y} mf(x, y)} \quad (9)$$

$$t' = t(x - u, y - v)mt(x - u, y - v) \quad (10)$$

$$\bar{t}' = \frac{\sum_{x,y} t'}{\sum_{x,y} mt(x - u, y - v)} \quad (11)$$

The numerator of Eq. (6) can be expanded as:

$$\lambda_{num} = \sum_{x,y} f' \cdot t' - \bar{f}'_{u,v} \sum_{x,y} t' - \bar{t}' \sum_{x,y} (f' - \bar{f}'_{u,v}) \quad (12)$$

In Eq. (11),  $\bar{t}'$  is a constant. Thus,  $t'$  can be transformed in advance to subtract the mean value of the valid data and let  $\bar{t}' = 0$ . For the sum of the pattern's valid data,  $\sum_{x,y} t'$ , it is invariable when the pattern is moving and can be pre-calculated. For the remainder of Eq. (11),  $\sum_{x,y} f' \cdot t'$  is the cross-correlation, which can be obtained using FFT for fast calculating.

The denominator of Eq. (6) is composed of two variance parts,  $f$  and  $t$ . For the part of  $t$ ,  $\sum_{x,y} (t' - \bar{t}')^2$ , the value is a constant, which can be pre-calculated. The part of  $f$ ,  $\sum_{x,y} (f' - \bar{f}'_{u,v})^2$ , can be decomposed as:

$$\sum_{x,y} (f' - \bar{f}'_{u,v})^2 = \sum_{x,y} (f')^2 - 2\bar{f}'_{u,v} \sum_{x,y} f' + \bar{f}'_{u,v}^2 \quad (7)$$

$$= \sum_{x,y} (f')^2 - \frac{(\sum_{x,y} f')^2}{\sum_{x,y} mf} \quad (12)$$

In the right side of Eq. (12), the three parts,  $(\sum_{x,y} f')^2$ ,  $\sum_{x,y} (f')^2$ , and  $\sum_{x,y} mf$ , must be re-calculated as the NCC window moves. Recalculating these matrices requires heavy computation that limits the applications of the NCC function. To simplify the calculation, Ref. [12] proposed the sum-table method to pre-calculate the denominator of the NCC function. This method significantly improved the computational efficiency. As a classical fast method, it was adopted widely in template matching applications. For VDNCC, the void points are assigned 0 after multiplying with the valid data templates and do not affect the sum calculation; thus, the sum-tables can also be applied to VDNCC. The sum-tables for VDNCC are expressed by:

$$s(u, v) = f(u, v)mf(u, v) + s(u - 1, v) + s(u, v - 1) - s(u - 1, v - 1) \quad (13)$$

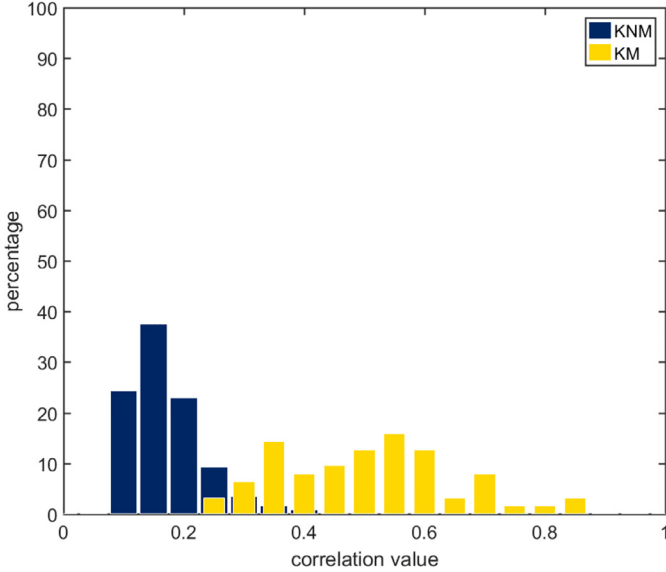


Fig. 14. Standard NCC matching results of breech face samples.

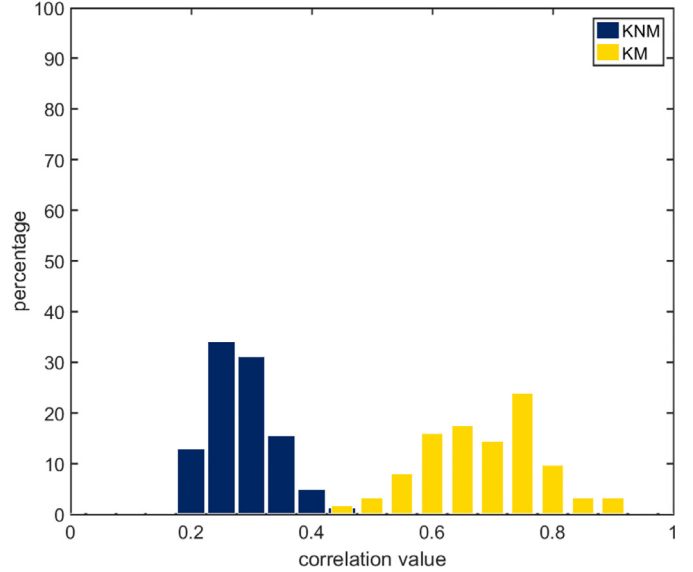


Fig. 16. VDNCC matching results of breech face samples.

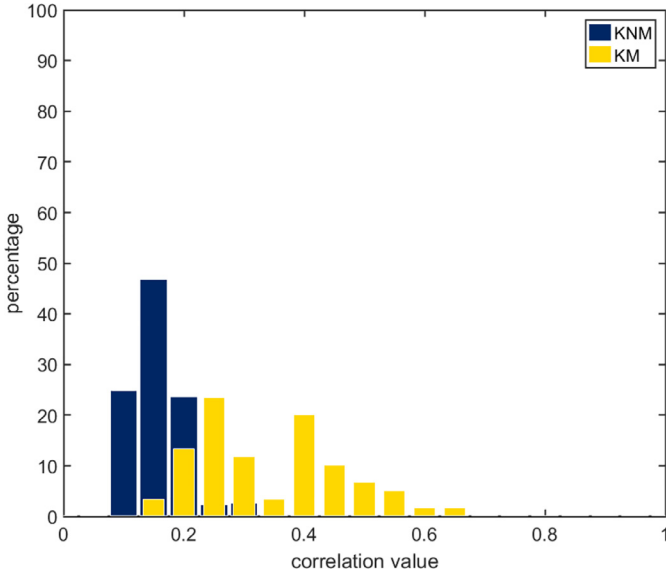


Fig. 15. Standard NCC matching results of firing pin samples.

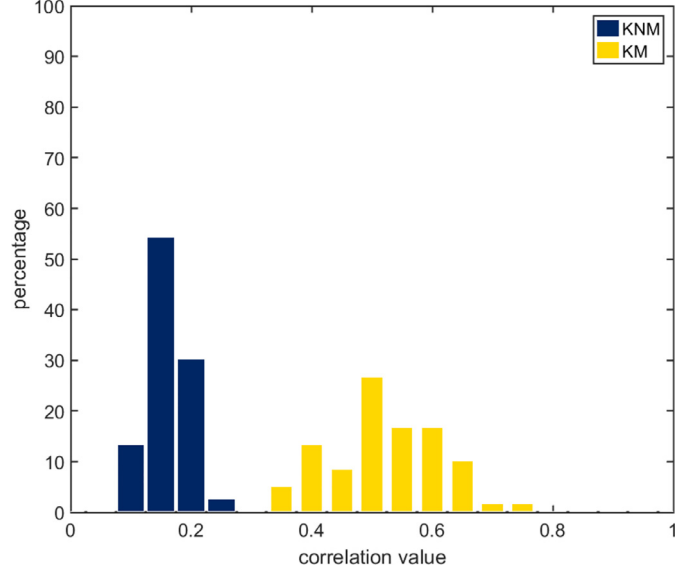


Fig. 17. VDNCC matching results of firing pin samples.

$$s^2(u, v) = [f(u, v)m_f(u, v)]^2 + s^2(u-1, v) + s^2(u, v-1) - s^2(u-1, v-1) \quad (14)$$

$$ms(u, v) = m_f(u, v) + ms(u-1, v) + ms(u, v-1) - ms(u-1, v-1) \quad (15)$$

Then, the accumulations can be deduced as:

$$\sum_{x,y} f' = s(u+N_x-1, v+N_y-1) - s(u-1, v+N_y-1) - s(u+N_x-1, v-1) - s(u-1, v-1) \quad (16)$$

$$\sum_{x,y} (f')^2 = s^2(u+N_x-1, v+N_y-1) - s^2(u-1, v+N_y-1) - s^2(u+N_x-1, v-1) - s^2(u-1, v-1) \quad (17)$$

$$\begin{aligned} \sum_{x,y} m_f &= ms(u+N_x-1, v+N_y-1) - ms(u-1, v+N_y-1) \\ &\quad - ms(u+N_x-1, v-1) - ms(u-1, v-1) \end{aligned} \quad (18)$$

## 5. Application of VDNCC in 3D ballistics identifications

### 5.1. Correlation tests of breech face and firing pin impressions

To test the effects of different NCC algorithms for ballistics identifications of breech face and firing pin impressions on primers of cartridge cases, a statistical study is performed. We select two sets of cartridge cases to test VDNCC. The first set is the 40 breech face impressions of the Fadul set [16], and the second set is the 40 firing pin impressions of the NBIDE set [6]. In each set, the 4 cases are from the same source. The raw impression surfaces are measured by the National Institute of Standards and Technology (NIST) using confocal microscopy and filtered using the isotropic areal spline filter to remove the large-scale distortions

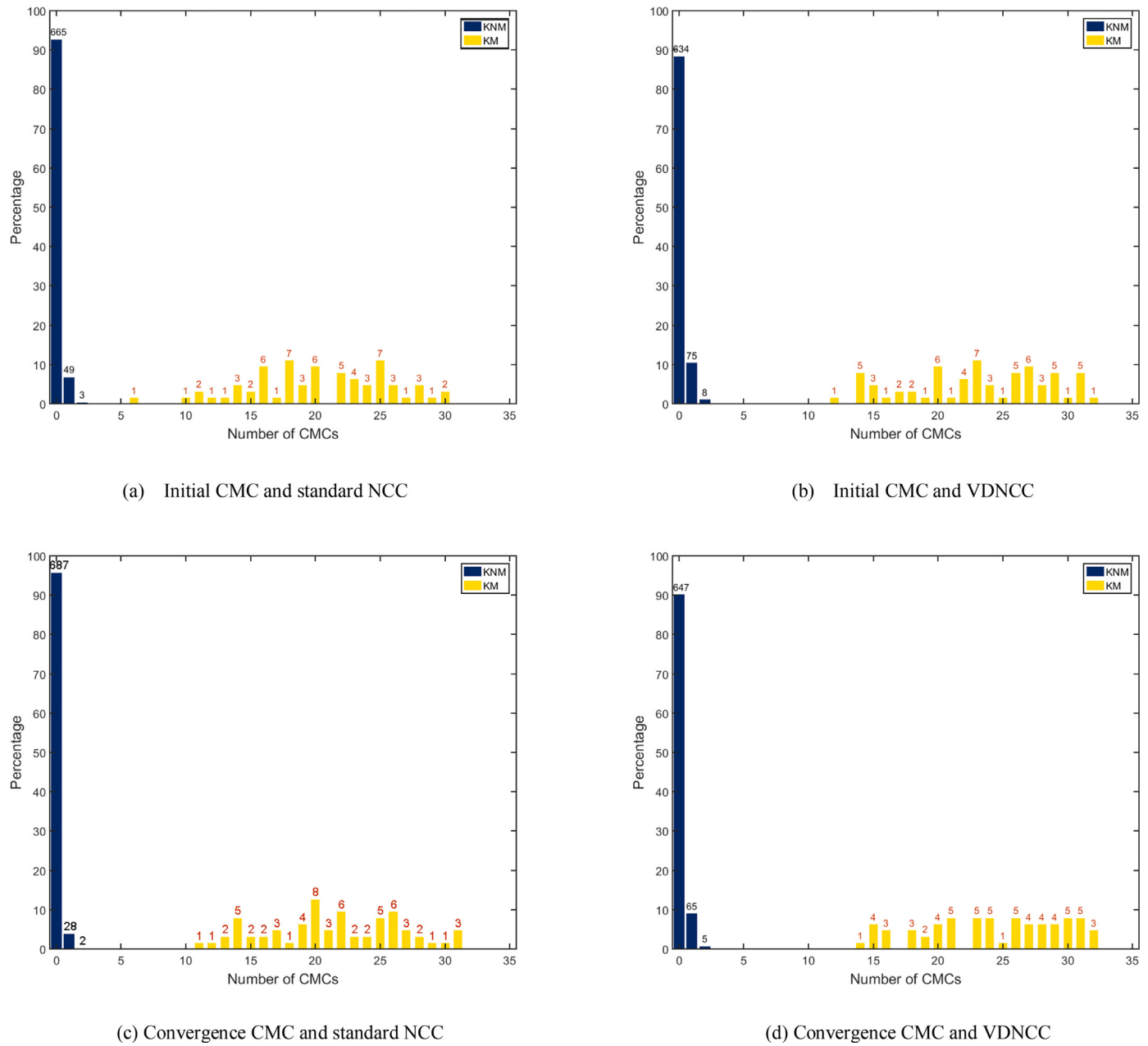


Fig. 18. CMC tests for the Fadul sample set based on different NCC algorithms.

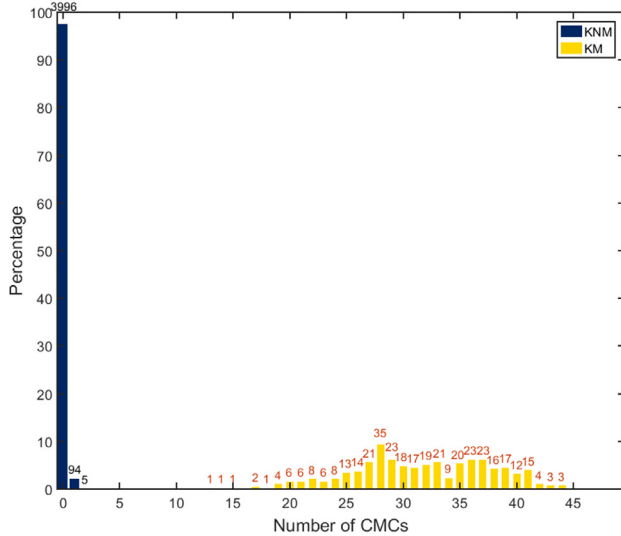
[15,17]. The typical data of the two ballistic sets are shown in Fig. 2. Each impression compared with the others generates 780 correlations, including 63 known-matching correlations (KM) and 717 known-non-matching correlations (KNM). The two full data are calculated using the standard NCC and VDNCC respectively. In each correlation, the reference impression is rotated with 3° step to ensure the KM correlation pair could identify the matching position, and the global maximum NCC of all rotations is recorded as the final matching score. Figs. 14 and 15 show the KM and KNM distributions of the Fadul set and the NBIDE set correlated by standard NCC. The overlaps of the two sets are 23.5% and 63.3%.

Performing the same tests using VDNCC, the results are shown in Figs. 16 and 17. The overlaps of the Fadul set and the NBIDE set are 1.4% and 0%, respectively. The decreased overlap indicates that the VDNCC can reduce the effects of the void area and improve the capability of the ballistics identification. In this test, both KNM distributions move different distances to the right due to the

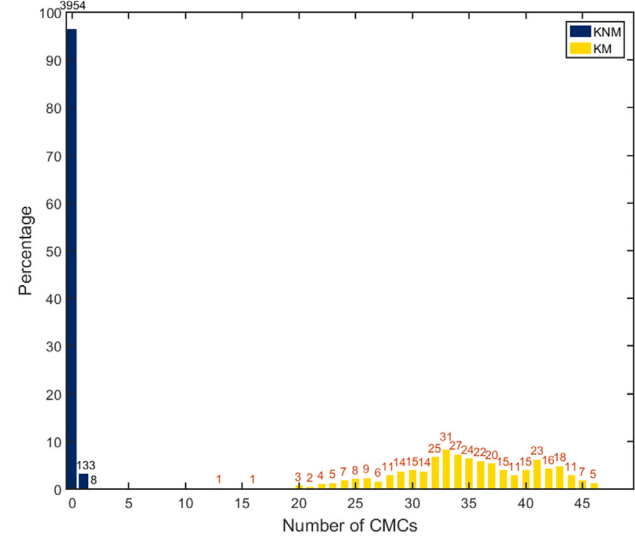
shapes of the void areas are different. As the two KNM breech face impressions in Fig. 2(a) and Fig. 12(b), the geometrical characteristics, such as the size and position, of the interior void area made by firing pin are various. The variant void areas are included in the standard NCC and result in the lower correlation score. For the firing pin impressions, the shape difference is minor and result in the two KNM distributions moving are unapparent.

## 5.2. Applications on the congruent matching cells (CMC) method

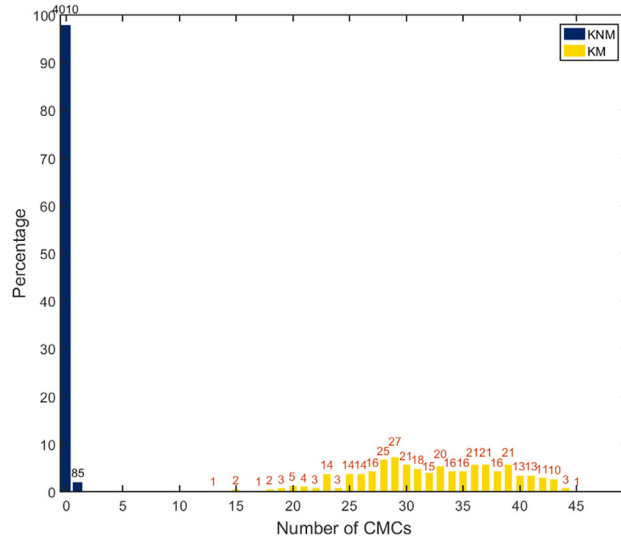
VDNCC can be used as a kernel evaluation algorithm in other ballistics identification methods. The CMC method proposed by NIST is an NCC based identification method [18]. The basic idea is to divide the measured image into small correlation cells so that “invalid” areas can be isolated from “valid” areas that contain unique identifying marks to improve correlation accuracy. In this method, the distribution of KM and KNM cell pairs for  $CCF_{max}$  (the kernel evaluation parameter of CMC method, equivalent to maxi-



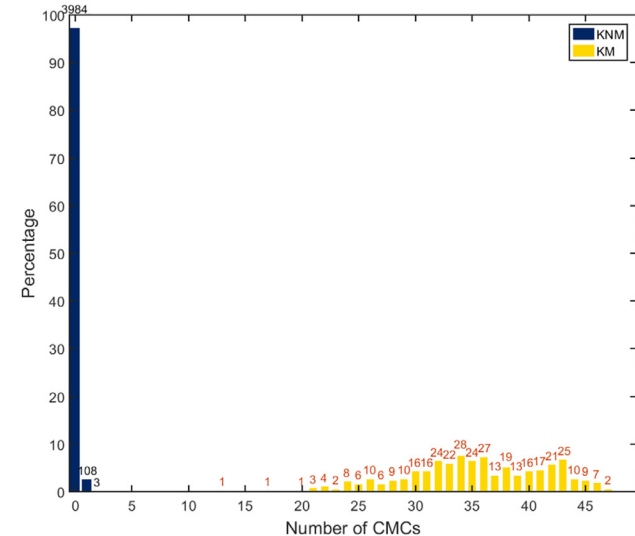
(a) Initial CMC and standard NCC



(b) Initial CMC and VDNCC



(c) Convergence CMC and standard NCC



(d) Convergence CMC and VDNCC

Fig. 19. CMC tests for the Weller sample set based on different NCC algorithms.

mum NCC score for each cell) is an important indicator to adjust the calculation parameters of the CMC method. The large overlap of this distribution “will involve a large error rate for both the false positive and the false negative errors” [19]. In this section, two sample sets of breech face impressions, which were used in the CMC study [20], are tested to verify the VDNCC algorithm. The first set is the Fadul set with 63 KM and 717 KNM, which is used in Section 5.1. The second set is the Weller set with 95 cartridge cases [10] and generates 370 KM and 4095 KNM.

The tests are based on the same processing as the initial CMC method and Convergence CMC method (the latest derivative algorithm) [20]. The only difference is that the calculation was based on standard NCC or VDNCC. Table 6 is the comparison of  $f_1$  (false identification rate) and  $f_2$  (false exclusion rate) of the  $CCF_{max}$ . The results show that the  $f_1$  and  $f_2$  of VDNCC are lower than standard NCC that could be conducive to reducing the error rate in the final CMC result. Figs. 18 and 19 are the CMC distributions based

**Table 6**  
Comparison of  $f_1$  and  $f_2$  of the  $CCF_{max}$ .

Sample set	Standard NCC		VDNCC	
	$f_1$	$f_2$	$f_1$	$f_2$
Fadul	11.43%	24.59%	10.65%	21.85%
Weller	7.5%	14.67%	5.54%	12.41%

on different NCC algorithms. The results show that the KM CMC distributions with VDNCC move significantly to the right in both sample sets, whether the calculations were based on the initial CMC method or the Convergence CMC method. The statistical results shown in Table 7 indicate that the mean values and median values of all KM groups increased about 3 CMCs, and the standard deviations had no significant difference. These test results indicate that VDNCC can improve the identification capability of the CMC method.

**Table 7**  
Statistical results of CMC test.

Test sample	Method	Mean value	Median value	S. D.
Fadul	Initial CMC & std. NCC	20.29	20	5.34
	Initial CMC & VDNCC	23.13	23	5.41
	Convergence CMC & std. NCC	2135	21	5.18
	Convergence CMC & VDNCC	24.22	24	5.27
Weller	Initial CMC & std. NCC	31.55	31.5	6.14
	Initial CMC & VDNCC	34.67	35	6.11
	Convergence CMC & std. NCC	32.27	32	6.31
	Convergence CMC & VDNCC	35.27	35	6.18

## 6. Conclusion

The void area will affect the results of the standard NCC function especially when the input data have changing regional mean values. The primary cause is that the filling value of the void area is not identically equal to the regional mean value. For ballistics identification, breech face impressions and firing pin impressions are both non-full filled matrices that may lead to adverse impacts for either KM matching or KNM matching based on the standard NCC function.

The proposed VDNCC function avoids the inclusion of the void area in the calculation and obtains a more objective similarity value. The experimental results show that the new algorithm can improve the capacity of ballistics identification in statistical tests of breech face and firing pin identifications. In the CMC test, VDNCC improved the correlation results in both the initial CMC and the derivative CMC algorithm, helped to reduce the error rates of both the false positive and the false negative errors and improved the identification capability. In conclusion, the VDNCC is a more objective and practical algorithm as a basic evaluation method for topography and image matching applications [19–21].

## Acknowledgment

The funding for this research is provided by National Natural Science Foundation of China (61703122, 61603113), National Postdoctoral Program for Innovative Talents (BX201600044), China Postdoctoral Science Foundation (2017M621259) and the 111 Project (B16014). The authors are grateful to the NIST researchers, Zhe Chen, Soons Johannes and John Song, for the valuable help.

## References

- [1] J. De Kinder, F. Tulleners, H. Thiebaut, Reference ballistic imaging database performance, *Forensic Sci. Int.* 140 (2) (2004) 207–215, doi:10.1016/j.forsciint.2003.12.002.
- [2] F. Xie, S. Xiao, L. Blunt, et al., Automated bullet-identification system based on surface topography techniques, *Wear* 266 (5) (2009) 518–522, doi:10.1016/j.wear.2008.04.081.
- [3] J. De Ceuster, S. Dujardin, The reference ballistic imaging database revisited, *Forensic Sci. Int.* 248 (2015) 82–87, doi:10.1016/j.forsciint.2014.11.025.
- [4] S. Yammen, P. Munesawang, Cartridge case image matching using effective correlation area based method, *Forensic Sci. Int.* 229 (1) (2013) 27–42, doi:10.1016/j.forsciint.2013.03.015.
- [5] W. Chu, R.M. Thompson, J. Song, T.V. Vorburger, Automatic identification of bullet signatures based on consecutive matching striae (CMS) criteria, *Forensic Sci. Int.* 231 (1) (2013) 137–141, doi:10.1016/j.forsciint.2013.04.025.
- [6] T.V. Vorburger, J.H. Yen, B. Bachrach, et al., Surface Topography Analysis for a Feasibility Assessment of a National Ballistics Imaging Database, National Institute of Standard and Technology, Gaithersburg (MD, 2007).
- [7] T.V. Vorburger, J. Song, N. Petracca, Topography measurements and applications in ballistics and tool mark identifications, *Surf Topogr: Metrol Prop.* 4 (1) (2015) 013002, doi:10.1088/2051-672X/4/1/013002.
- [8] M. Tong, J. Song, W. Chu, R.M. Thompson, Fired cartridge case identification using optical images and the congruent matching cells (CMC) method, *J. Res. Natl. Inst. Stan.* 119 (2014) 575–582, doi:10.6028/jres.119.023.
- [9] N. Senin, R. Groppetti, L. Garofano, et al., Three-dimensional surface topography acquisition and analysis for firearm identification, *J. Forensic Sci.* 51 (2) (2006) 282–295, doi:10.1111/j.1556-4029.2006.00048.x.
- [10] T.J. Weller, A. Zheng, R. Thompson, F. Tulleners, Confocal microscopy analysis of breech face marks on fired cartridge cases from 10 consecutively manufactured pistol slides, *J. Forensic Sci.* 57 (4) (2012) 912–917, doi:10.1111/j.1556-4029.2012.02072.x.

- [11] C. Gambino, P. McLaughlin, L. Kuo, et al., Forensic surface metrology: tool mark evidence, *Scanning* 33 (5) (2011) 272–278, doi:10.1002/sca.20251.
- [12] J.P. Lewis, Fast normalized cross-correlation, *Vis. Interface* 10 (1) (1995) 120–123.
- [13] K. Briechle, U.D. Hanebeck, Template matching using fast normalized cross correlation, *Proc. SPIE* 4387 (2001) 95–102, doi:10.1117/12.421129.
- [14] MathWorks Inc., Normxcorr2, Available at: <https://cn.mathworks.com/help/images/ref/normxcorr2.html>. (Accessed 25 June 2017)
- [15] M. Tong, H. Zhang, D. Ott, et al., Applications of the spline filter for areal filtration, *Meas. Sci. Technol.* 26 (12) (2015) 127002, doi:10.1088/0957-0233/26/12/127002.
- [16] T.G. Fadul Jr, G.A. Hernandez, S. Stoiloff, et al., An Empirical Study to Improve the Scientific Foundation of Forensic Firearm and Tool Mark Identification Utilizing Consecutively Manufactured Slides, US Department of Justice, National Institute of Justice, Washington, DC, 2011.
- [17] M. Tong, H. Zhang, D. Ott, et al., Analysis of the boundary conditions of the spline filter, *Meas. Sci. Technol.* 26 (9) (2015) 095001, doi:10.1088/0957-0233/26/9/095001.
- [18] J. Song, W. Chu, M. Tong, et al., 3D topography measurements on correlation cells—a new approach to forensic ballistics identifications, *Meas. Sci. Technol.* 25 (6) (2014) 064005, doi:10.1088/0957-0233/25/6/064005.
- [19] W. Chu, M. Tong, J. Song, Validation tests for the congruent matching cells (CMC) method using cartridge cases fired with consecutively manufactured pistol slides, *AFTE J.* 45 (4) (2013) 361–366.
- [20] Z. Chen, J. Song, W. Chu, et al., A convergence algorithm for correlation of breech face images based on the congruent matching cells (CMC) method, *Forensic Sci. Int.* 280 (2017) 213–223, doi:10.1016/j.forsciint.2017.08.033.
- [21] W. Lin, X. Ren, T. Zhou, et al., A novel robust algorithm for position and orientation detection based on cascaded deep neural network, *Neurocomputing* (2018), doi:10.1016/j.neucom.2018.04.061.



**Mingsi Tong** received his Ph.D. degree in mechatronic engineering from Harbin Institute of Technology, Harbin, China, in 2016. During graduate period, he also concurrently studied in the National Institute of Standards and Technology, DC, USA, as a Guest Researcher. He is currently an assistant Professor in the School of Mechatronics Engineering, Harbin Institute of Technology. His research interests include forensic science, pattern recognition, surface metrology.



**Yunlu Pan** received the Bachelor and M.Sc. degree in Mechanical Engineering from Harbin Institute of Technology, China, in 2008 and 2010 respectively; and the Ph.D. degree in Mechatronics engineering from Harbin Institute of Technology, China, in 2014. Currently, he is an Associate Professor in the School of Mechatronics, Harbin Institute of Technology. His research interests include superwetting surfaces and their applications, micro/nano sensors.



**Zhan Li** received his Ph.D. degree in control science and engineering from Harbin Institute of Technology, Harbin, China, in 2015. He received his B.Sc. degree in automation, and the Master's degree in pattern recognition and intelligent system, from Harbin Engineering University, Harbin, China, in 2008 and 2011, respectively. From 2013 to 2014, he was visiting University of Toronto Institute for Aerospace Studies (UTIAS), Toronto, Canada, as a joint PhD student supported by China Scholarship Council (CSC), working with co-advisor Prof. Hugh Liu. He is currently a lecturer at the School of Astronautics, Harbin Institute of Technology. His current research interests include motion control, industrial robot control, robust control of small UAVs, and cooperative control of multi-vehicle systems.



**Weiyang Lin** received the Bachelor and M.Sc. degree in Mechanical Engineering from Harbin Institute of Technology, China, in 2006 and 2008 respectively; and the Ph.D. degree in Mechatronics engineering from Harbin Institute of Technology Shenzhen Graduate School, China, in 2014. Currently, he is an Assistant Professor in the Research Institute of Intelligent Control and Systems, Harbin Institute of Technology. His research interests include parallel manipulators, robotic motion control and medical robotic design and control.